

Eddy-current tunnel magnetic contacts with a composite free layer

© I.Yu. Pashenkin,¹ E.V. Skorokhodov,¹ M.V. Sapozhnikov,^{1,2} A.A. Fraerman,¹ G.A. Kichin,³ K.A. Zvezdin^{3,4}

¹Institute for Physics of Microstructures, Russian Academy of Sciences, branch of the Federal Research Center „Institute of Applied Physics of the Russian Academy of Sciences“, 603087 Nizhny Novgorod, Russia

²Lobachevsky State University, 603950 Nizhny Novgorod, Russia

³New Spintronic Technologies, Russian Quantum Centre, Skolkovo Innovation Center, 121205 Moscow, Russia

⁴Prokhorov Institute of General Physics, Russian Academy of Sciences, 119991 Moscow, Russia
e-mail: evgeny@ipmras.ru

Received July 7, 2023

Revised September 14, 2023

Accepted September 25, 2023

A new method was offered to design tunnel magnetoresistive CoFeB/MgO/CoFeB contacts with free layer vortex magnetization configuration. Contacts are made using electron-beam lithography methods and have lateral sizes of ~ 700 nm. The achieved tunnel magnetoresistance effect was equal to 80–120% for various samples. Thanks to low coercitivity, the magnetoresistance curve has a linear section without magnetic hysteresis that corresponds to vortex offset from the central position. Such types of contacts show spin-transfer diode properties — they feature rectification of high-frequency signals on vortex magnetization configurations.

Key words: magnetic tunnel contacts, spin-transfer diode effect, vortex spin-transfer nanooscillators.

DOI: 10.61011/TP.2023.11.57501.171-23

Introduction

Possibility of vortex magnetization distribution in magnetic nanoparticles was experimentally demonstrated in the late 1990s [1,2]. This magnetization distribution corresponds to the minimum of magnetostatic energy where scattering fields are absent. Vortex state features its linear response to external magnetic field [1] and low frequency of the fundamental (gyrotropic) magnetization oscillation mode that, among other things, depends on the magnetic particle size [3] and may be easily changed. One of the promising practical applications of magnetic vortex states is the production of tunnel magnetic contacts with vortex magnetization distribution.

Magnetic tunnel contacts are a multilayer structure consisting of ultrathin insulating layer (serving as a tunnel barrier) between two ferromagnetic (FM) layers. One of the FM layers has fixed magnetic orientation and is referred to as a reference layer (RL) and the other FM layer is referred to as a free layer (FL) and has magnetic orientation that may be both parallel and antiparallel to the RL magnetization. Tunnel magnetoresistance effect (TMR effect) of the tunnel contact may achieve 600% in case of MgO barrier [4]. It should be noted that the TMR contact stack composition in real practice, as discussed below, may be also more complex and include composite ferromagnetic layers, artificial antiferromagnetic materials, and pinning layers made of real antiferromagnetic substances such as IrMn, however, for the sake of simplicity we restrict the

description to a three-layer TMR contact model. In vortex tunnel contacts, FL has vortex magnetic state and RL is uniformly magnetized. System resistance changes when the magnetic vortex is offset from the equilibrium position in the FL center. Currently, three main spintronics development areas may be distinguished where TMR vortex contact applications have the particular potential. First, this is the development of high-sensitivity magnetic field TMR sensors [5,6]. The vortex state advantage here is in its linear unhysteretic response to external magnetic field. Sensitivity of such sensors may easily achieve 0.1%/Oe [5]. The second vortex TMR contact application area — in the development of co-called spin-transfer nanooscillators that are compact VHF radiation sources [7–10]. Their operating principle consists in excitation of gyrotropic self-oscillations of free-layer magnetic vortex when DC current flows through a tunnel contact. Excitation performance of such oscillations is associated with high degree of spin current polarization in the contact. Inverse effect, i.e. occurrence of continuous current when variable VHF voltage is applied to a vortex TMR contact, is referred to as spin-transfer diode effect. It is expected to be successfully used to extract energy from non-equilibrium variable electric fields that exist in the process environment [11,12]. This so-called „electromagnetic harvesting“ may be provided at the incoming power of about $1 \mu\text{W}$ and lower [13].

Simultaneous implementation of low-coercive vortex free-layer state and strong TMR effect in a single TMR contact is a prerequisite of successful operation of such

devices. By now, the highest TMR effect is observed in CoFeB/MgO/CoFeB TMR contacts with crystal texture with orientation [001] [4], because additional spin filtration of tunneling electrons in MgO layer is provided in this case [14]. Such contacts are made by magnetron sputtering followed by magnetic field annealing at $\sim 300^\circ\text{C}$. Annealing serves to provide crystallization of initially amorphous CoFeB layers from initially textured MgO layer. A polycrystalline texture of the CoFeB layer improves magnetic layer coercivity, as a result of which magnetic vortex is either not implemented during remagnetization or the vortex core becomes heavily pinned at random pinning centers. In both cases, the TMR contact loses its advantages associated with vortex magnetization distribution, i.e. with linear unhysteretic response.

If FL is made from, for example, NiFe, rather than from a textured CoFeB layer, as specified in [11], then low-coercive magnetic vortex state is implemented in the free layer, but the observed effect size is much lower — only 8.5%. To avoid this problem, the following method was used in the studies quoted above. During sputtering, composite FL was produced of several different layers with CoFeB/Ru/NiFe [6], CoFe/CoFeB/NiFe/Co/Cu/[Co/Ni]10 structure [8]. The presence of thin intermediate metallic non-magnetic layer is a significant feature of the specified structures ($\sim 1\text{ nm}$). It serves to provide crystallization and texturing of the initially amorphous free magnetic layer during annealing process ($\sim 330^\circ\text{C}$) only from the interface with the MgO dielectric barrier, rather than from the interface with the NiFe layer. Whereby the lower textured CoFeB sublayer provides the required spin filtration of tunneling electrons and high TMR effect (100–200%), and the NiFe layer provides vortex magnetization distribution of the exchange-coupled FL structure.

Disadvantage of this system is in the requirement to use additional materials (and, thus, a larger amount of magnetrons) during magnetron sputtering and to implement accurate control of additional layer thickness to ensure magnetic exchange between two magnetic sublayers of the free layer.

This study uses an alternative original method of vortex TMR contact production that does not use layers of additional materials, and demonstrates the presence of spin-transfer diode effect in the prepared structures.

1. Study objects

Multilayer nanostructures with functional IrMn(10)/CoFeB^T(3–5)/MgO(1–1.5)/CoFeB^T(5–7)/CoFeB^A(40–50) layers were used as basis for production of vortex TMR components. Thicknesses are given in nanometers and may differ for different structures. „T“ and „A“ indices mean „textured“ and „amorphous“, respectively. antiferromagnetic IrMn layer serves to fix magnetization of the lower magnetic layer due to pinning, the functional upper layer has a composite structure consisting of a lower textured thin

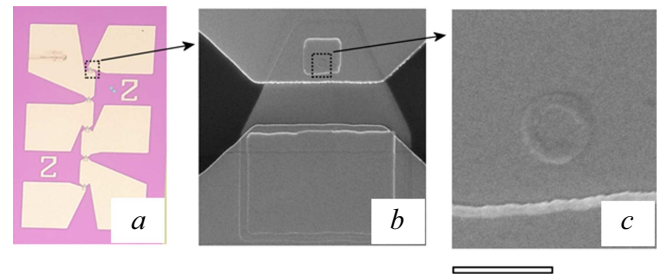


Figure 1. *a* — image of serial chain of five successive TMR contacts in the optical microscope. Frame width is 0.5 mm; *b, c* — gradually magnified images of an individual TMR contact in the electron microscope. Size of the mark in *c* corresponds to 1 μm .

sublayer that ensures effective spin filtration of the flowing current and high TMR effect (up to 100–200% for our samples) and an upper thick amorphous layer thanks to which weakly pinned vortex magnetization distribution is formed in the TMR contact. For CoFeB layer texturing, annealing at 300°C is required. Therefore, formation of the structure consists of two stages. First, a thin upper CoFeB layer was deposited in a magnetron unit and was covered with a Pt layer. Then annealing was carried out in a separate chamber for texturing CoFeB layers, after which the sample was returned into the magnetron unit, the protective Pt layer was removed by ion etching method, and then a 40 nm amorphous CoFeB layer was grown on the textured CoFeB layer. Actually, the upper magnetic layer may be made from any low-coercive magnetic material, e.g. NiFe. The benefit of amorphous CoFeB is the fact that it has low coercivity and low ferromagnetic resonance attenuation coefficient compared with NiFe [15], but has higher magnetization that facilitates formation of vortex distribution. It should be noted that, if the sputtering magnetron unit allows sputtering and magnetic field annealing to be performed simultaneously, then the additional Pt layer sputtering operation (required for protection against oxidation during annealing in a separated unit) may be avoided, and sputtering of the upper composite free magnetic CoFeB layer may be carried out as a single process in two stages with intermediate annealing. Multilayer nanostructures for production of TMR contacts were formed by high vacuum magnetron sputtering on Si/SiO₂ substrate. TMR structure sputtering conditions are described in detail in [16,17].

Multilayer TMR structures were used for next TMR contact production process operations. Nanocontact was made from the TMR structure by the electron-beam lithography method followed by ion etching in resistive mask. The contact area had a round cylindrical shape (Figure 1, *c*) with a typical size of 700 nm. Lead contacts and terminal pads were made by maskless photolithography. Each sample accommodated 5 individual TMR contacts (Figure 1, *a*). Connector pin assignment enabled measurements to be carried out both on individual TMR contacts and on entire chain of 5 serial contacts. The samples designed for VHF

The resistance values of the samples under study (correspond to curves in Figure 2)

Curve	TMR contact free layer structure	Magnetic configuration of the free layer	R_{\min} (k Ω)	R_{\max} (k Ω)	TMR
<i>a</i>	Amorphous	Vortex	8.65	9.24	7%
<i>b</i>	Textured	quasi-homogeneous	31.16	65.1	109%
<i>c</i>	Composite	Vortex	10.45	4.76	120%

measurements were made with resistance probably closer to 50 Ω for better coordination. We were able to make TMR contacts 700 nm in diameter with resistance 250–500 Ω , corresponding MgO layer thickness is \sim 1.2 nm. It should be noted that the contacts with such low resistance had the TMR effect reduced to 80–100% compared with maximum achieved 200% at MgO thicknesses of 1.5–1.6 nm. This is due to lower spin filtration at low barrier thicknesses and to higher shunting effect, lead contact resistance contribution.

2. Measurement of transport properties

Measurements of static transport properties of TMR contacts were carried out using probe station in magnetic fields up to 600 Oe. These measurements were performed mainly for a chain of contacts in order to reduce the probability of accidental static breakdown, because the resistance of a single contact is quite low. Typical kinds of magnetoresistance loops obtained for the contact chains are shown in Figure 2. The results are given in relative units for better comparison. Absolute maximum and minimum resistances are listed in the Table. Addition to resistance as a result of magnetization disorientation in free and fixed layers is assessed as

$$\Delta R \sim \int_S M_1 M_2 dS \sim \langle M_{2x} \rangle,$$

where M_1 and M_2 — are free and fixed layers magnetizations, and x is the fixed layer magnetization orientation that is assumed as homogeneous. Thus, the magnetoresistance waveform corresponds to the free-layer magnetization waveform to a good approximation. It is shown that the initial unannealed TMR contact (Figure 2, *a*) demonstrates the magnetoresistance curve typical for the vortex magnetization distribution [5] in the free layer. However, the TMR effect is only 7%, because the amorphous CoFeB layers do not provide high spin polarization of electrons with wave vectors perpendicular to the barrier. TMR contact annealing resulted in the increase in the TMR effect up to 109%, but the loop form changed considerably that is indicative of high pinning of the vortex core on the polycrystalline structure of the textured CoFeB layer. As a result a narrow ligament on the curve in the zero field disappears and

the hysteresis becomes wide. If CC has a composite structure consisting of textured and amorphous CoFeB layers, then such contact demonstrates simultaneously high TMR effect (120%) and a hysteresis curve typical for the vortex magnetization distribution with a narrow ligament in the zero field (Figure 2, *c*). It should be emphasized that, if the magnetic field variation range is lower than the critical field of magnetic vortex exit from the free layer, then the TMR effect curve has a linear unhysteretic form (Figure 2, *d*) that is precisely as required for possible development of magnetic field sensors. Sensitivity in this case is 0.1%/Oe (1 mV/V/Oe) in the field range \pm 100 Oe.

Since individual contacts in the chain have a little different parameters, this results in some broadening of the curves compared with the behavior that shall be demonstrated by single contacts. Nevertheless, the magnetoresistance curve with the ligament in the center (Figure 2, *c*) typical for the vortex magnetization distribution is clearly observed.

3. Measurement of spin-transfer diode effect

Additionally in the prepared samples, the spin-transfer diode effect was investigated, that involved occurrence of DC voltage during VHF current flow through the TMR contact. Such rectification effect is observed in the TMR contacts and is associated with the resonance excitation of gyrotropic magnetic vortex oscillations due to the flowing AC spin-polarized current. Vortex position oscillations result in resistance oscillations in the whole structure at the same frequency as the VHF current frequency. As a result, quadratic nonlinear occurs and results to the occurrence of constant difference of potentials on contacts. The resistance oscillation amplitude and the DC voltage are proportional to the gyrotropic oscillation vortex amplitude and depend on the AC frequency in a resonant manner.

The experiment setup is shown in Figure 3, *a*. AC current was generated by the VHF oscillator (NI PXIe-5652) and applied to the TMR sample through a bias-tee (bias-T). Simultaneously, the rectified output voltage was measured using a source-meter (NI PXIe-4139). VHF current frequency varied in the range from 200 to 500 MHz, the maximum current power was equal to 1.6 mW (2 dBm). Dependences of the rectified voltage on the frequency for various applied magnetic field values are shown in Figure 3, *b*. Rectification spectra shapes and resonance frequencies within the subgigahertz range indicate that free-layer vortex magnetic configuration is observed in the samples. Such behavior and typical resonance frequencies agree with the theoretical model shown in [18]. The experiment shows that for the field of 110 Oe resonant rectification occurs at 305 MHz. When the field increases, the resonance moves towards higher frequencies and, when the field is 163 Oe, the resonant rectification is observed as early as at 345 MHz. Then the resonance moves back towards low frequencies and, when the field is 205 Oe, the

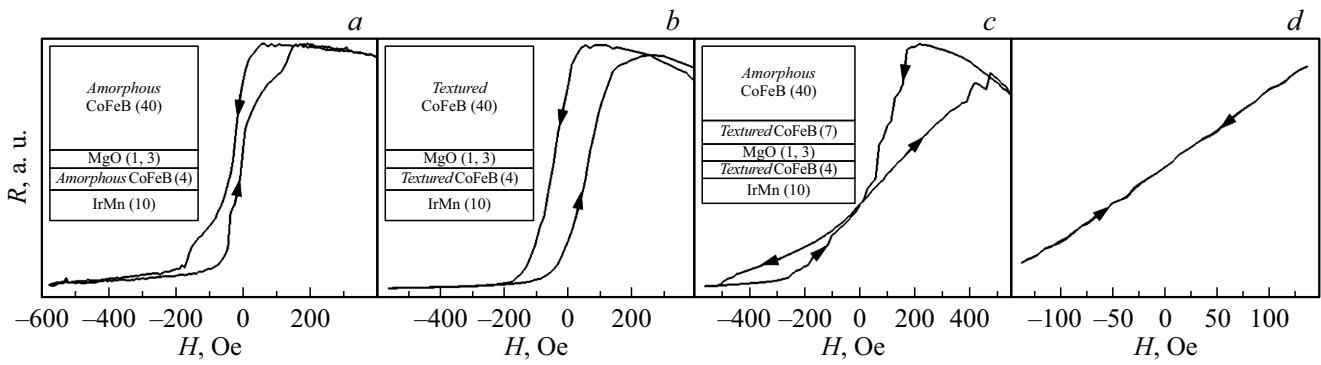


Figure 2. magnetoresistance curves of TMR contact chains with different layer structures. Details schematically show the corresponding structures. *a* — TMR contact with both amorphous magnetic layers (before annealing), TMR effect is 7%; *b* — the same TMR contacts after annealing with both textured magnetic layers, TMR effect is 109%; *c* — contact with composite FL, TMR effect is 120%; *d* — linear unhysteretic section of the curve shown in Figure 2, *c*.

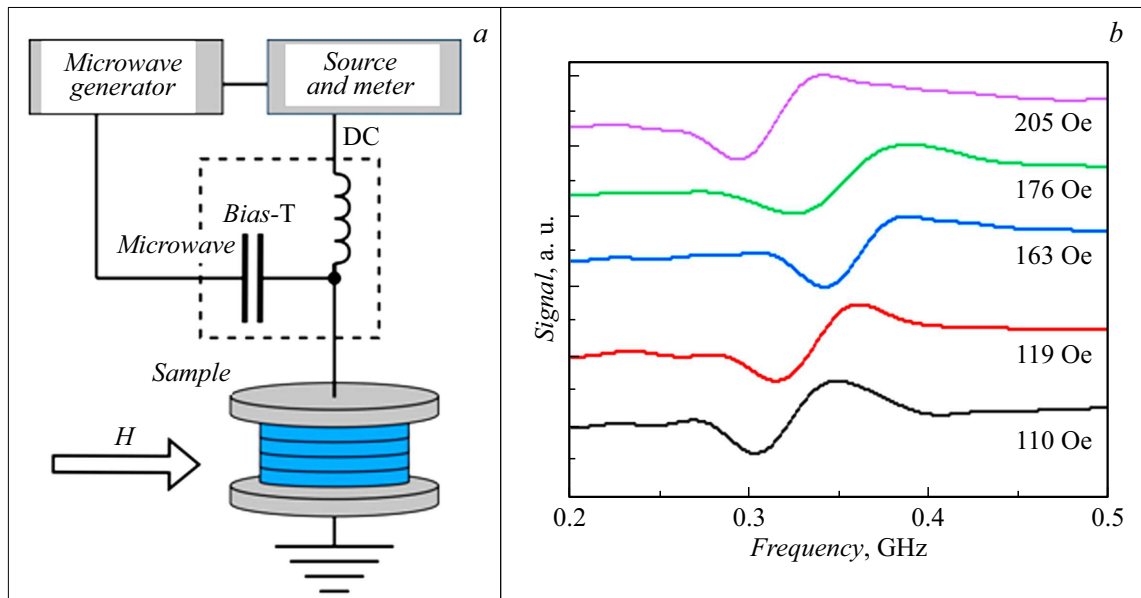


Figure 3. *a* — experiment setup for investigation of spin-transfer diode effect in the TMR contacts; *b* — rectified DC voltage on the TMR contact vs. AC frequency.

resonant frequency is 295 MHz. The maximum rectified voltage is 5 mV at the VHF pumping power of 1.6 mW (2 dBm). Resonant frequencies and resonant frequency dependence on the applied magnetic field (Figure 3, *c*) are also typical for gyrotropic magnetic vortex oscillations.

Conclusion

thus, the paper offers an original method for production of TMR contacts on the basis of CoFeB/MgO/CoFeB structure with vortex magnetization distribution in FL. The produced TMR contacts demonstrate maximum TMR value of 200%, but effective rectification of HF signals is observed even at TMP 80–100%. The samples demonstrate a linear unhysteretic response to the external magnetic field. The presence of strong spin-transfer diode effect has been

demonstrated suggesting that the produced TMR contacts may be used as magnetic field sensors.

Funding

Development of the vortex TMR contact production process and AC investigations were supported by the RSF grant (21-12-00271), VHF measurements were supported by the RSF grant (19-12-00432).

Conflict of interest

The authors declare that they have no conflict of interest.

References

- [1] R.P. Cowburn, D.K. Koltsov, A.O. Adeyeye, M.E. Welland, D.M. Tricker. *Phys. Rev. Lett.*, **83**, 1042 (1999). DOI: 10.1103/PhysRevLett.83.1042
- [2] T. Okuno, K. Shigeto, T. Ono, K. Mibu, T. Shinjo. *Sci.*, **240**, 1 (2002). DOI: 10.1126/science.289.5481.930
- [3] K.A. Zvezdin, E.G. Ekomasov. *Fizika metallov i metallovedenie*, **123**, 219 (2022) (in Russian). DOI: 10.31857/S0015323022030147
- [4] S. Ikeda, J. Hayakawa, Y. Ashizawa, Y.M. Lee, K. Miura, H. Hasegawa, M. Tsunoda, F. Matsukura, H. Ohno. *Appl. Phys. Lett.*, **93**, 082508 (2008). DOI: 10.1063/1.2976435
- [5] G. He, Y. Zhang, G. Xiao. *Phys. Rev. Appl.*, **14**, 034051 (2020). DOI: 10.1103/PhysRevApplied.14.034051
- [6] M. Endo, M. Al-Mahdawi, M. Oogane, Y. Ando. *J. Phys. D: Appl. Phys.*, **55** (19), 195001 (2022). DOI: 10.1088/1361-6463/ac5080
- [7] A. Dussaux, B. Georges, J. Grollier, V. Cros, A.V. Khvalkovskiy, A. Fukushima, M. Konoto, H. Kubota, K. Yakushiji, S. Yuasa, K.A. Zvezdin, K. Ando, A. Fert. *Nat Commun.*, **1**, 8 (2010). DOI: 10.1038/ncomms1006
- [8] A. Dussaux, E. Grimaldi, B.R. Salles, A.S. Jenkins, A.V. Khvalkovskiy, P. Bortolotti, J. Grollier, H. Kubota, A. Fukushima, K. Yakushiji, S. Yuasa, V. Cros, A. Fert. *Appl. Phys. Lett.*, **105**, 022404(2014). DOI: 10.1063/1.4885537
- [9] R. Lebrun, S. Tsunegi, P. Bortolotti, H. Kubota, A.S. Jenkins, M. Romera, K. Yakushiji, A. Fukushima, J. Grollier, S. Yuasa, V. Cros. *Nat. Commun.*, **8**, 15825 (2017). DOI: 10.1038/ncomms15825
- [10] A.S. Jenkins, L. San Emeterio Alvarez, P.P. Freitas, R. Ferreira. *Sci. Rep.*, **10**, 11181 (2020). DOI: 10.1038/s41598-020-68001-6
- [11] A.S. Jenkins, R. Lebrun, E. Grimaldi, S. Tsunegi, P. Bortolotti, H. Kubota, K. Yakushiji, A. Fukushima, G. de Loubens, O. Klein, S. Yuasa, V. Cros. *Nature Nanotech.*, **11**, 360 (2016). DOI: 10.1038/nnano.2015.295
- [12] P.N. Skirdkov, K.A. Zvezdin. *Ann. Phys.*, **532**, 1900460 (2020). DOI: 10.1002/andp.201900460
- [13] B. Fang, M. Carpentieri, S. Louis, V. Tiberkevich, A. Slavin, I.N. Krivorotov, R. Tomasello, A. Giordano, H. Jiang, J. Cai, Y. Fan, Z. Zhang, B. Zhang, J.A. Katine, K.L. Wang, P.K. Amiri, G. Finocchio, Z. Zeng. *Phys. Rev. Appl.*, **11**, 014022 (2019). DOI: 10.1103/PhysRevApplied.11.014022
- [14] W.H. Butler, X.-G. Zhang, T.C. Schulthess, J.M. MacLaren. *Phys. Rev. B*, **63**, 054416 (2001). DOI: 10.1103/PhysRevB.63.054416
- [15] C. Wang, Y.-T. Cui, J.Z. Sun, J.A. Katine, R.A. Buhrman, D.C. Ralph. *Phys. Rev. B*, **79**, 224416 (2009). DOI: 10.1103/PhysRevB.79.224416
- [16] I.Yu. Pashen'kin, M.V. Sapozhnikov, N.S. Gusev, V.V. Rogov, D.A. Tatarskiy, A.A. Fraerman. *Tech. Phys.*, **64**, 1642 (2019). DOI: 10.1134/S1063784219110227
- [17] I.Yu. Pashen'kin, M.V. Sapozhnikov, N.S. Gusev, V.V. Rogov, D.A. Tatarskii, A.A. Fraerman, M.N. Volochaev. *Pis'ma v ZhETF* **111**, 815 (2020). (in Russian). DOI: 10.31857/S1234567820120058
- [18] P.N. Skirdkov, A.F. Popkov, K.A. Zvezdin. *Appl. Phys. Lett.*, **113**, 242403 (2018). DOI: 10.1063/1.5064440

Translated by Ego Translating